

Ultrafast Gyroscopic Measurements in a Passive All-Fiber Mach–Zehnder Interferometer via Time-Stretch Technique

Igor Kudelin,* Srikanth Sugavanam, and Maria Chernysheva*

Almost all inertial navigation systems rely on optical gyroscopes, operating on the Sagnac effect. Laser gyroscopes demonstrate high precision in demanding applications such as seismology and geodesy. Passive optical gyroscopes, typically fiber-optic gyroscopes (FOGs), are of particular interest due to the lack of the “lock-in” effect, which is the most detrimental effect in active laser systems. Still, the current data acquisition rate of modern FOGs cannot satisfy emerging applications, particularly for autonomous navigation. Herein, a novel interferometric FOG, based on the measurements of ultrashort pulse phase via the dispersive Fourier transformation, is presented, demonstrating the highest up-to-date acquisition rate of 15 MHz. This setup is insensitive to the timing jitter and the fluctuations of the carrier-envelope phase of the pulses. The single-shot resolution of the phase retrieval is 7.3 mrad, which corresponds to a time shift of 8.7 attoseconds. As a confirmation of the high-speed performance, movements of a stepper motor are recorded with an angular velocity resolution of 0.33 mdeg s⁻¹ and a bias instability of 0.06 deg h⁻¹ at acquisition time of 17.07 μs. The proposed method can facilitate various phase measurements at a high repetition rate and is not limited only to gyroscopic applications.

offset of oscillation frequencies. Active gyroscopes are based on a bidirectional laser cavity, maintaining generation in counterpropagating directions. Commonly, detection of the Sagnac effect in active laser gyroscopes is based on the measurement of the beat-note frequency, corresponding to the offset of the counterpropagation oscillation frequencies. This method provides the highest resolution that comes at the cost of significant integration time. Moreover, at low angular velocities, active laser gyroscopes suffer from the so-called “lock-in” effect when the counterpropagating oscillating frequencies are synchronized due to backscattering.^[4] This deleterious effect could be eliminated in passive gyroscopes, i.e., interferometers without an active media. Such devices measure the Sagnac effect as a phase shift between counterpropagating pulses. The niche of passive gyros is occupied mainly by fiber-optic gyroscopes (FOGs). Another FOG’s benefits

1. Introduction

Optical gyroscopes are essential tools in inertial navigation and geophysical applications. Their extremely high precision has been proven by accurate measurements of seismic activities,^[1] the Chandler and annual wobbles of the Earth rotation axis.^[2] The operational principle of optical gyroscopes is based on the Sagnac effect,^[3] which is manifested as a time retardation between counterpropagated beams, leading to a phase shift or

is the possibility to multiply the overall sensitivity to the angular motion by coiling long optical fiber multiple times while preserving the small size of the device.

A newly emerged field of gyroscopic measurements is based on exploiting ultrafast lasers.^[5,6] The motivation for using new laser properties is driven by the substantially decreased “lock-in” effect in ultrafast lasers owing to small spatial interaction length.^[7] Furthermore, the intensity of the backscattered light is further reduced in such laser configurations due to the inherent properties of an intracavity intensity-discriminating

I. Kudelin
Aston Institute of Photonic Technologies
Aston University
Birmingham B4 7ET, UK
E-mail: Igor.Kudelin@colorado.edu

I. Kudelin
Department of Physics
University of Colorado
2000 Colorado Ave., Boulder, CO 80309, USA

 The ORCID identification number(s) for the author(s) of this article can be found under <https://doi.org/10.1002/adpr.202200092>.

© 2022 The Authors. Advanced Photonics Research published by Wiley-VCH GmbH. This is an open access article under the terms of the Creative Commons Attribution License, which permits use, distribution and reproduction in any medium, provided the original work is properly cited.

DOI: 10.1002/adpr.202200092

I. Kudelin
Time and Frequency Division
NIST
325 Broadway, Boulder, CO 80305, USA

S. Sugavanam
School of Computing and Electrical Engineering
IIT Mandi
Kamand 175075, Himachal Pradesh, India

M. Chernysheva
Leibniz Institute of Photonic Technology
Albert-Einstein-Str. 9, 07745 Jena, Germany
E-mail: Maria.Chernysheva@leibniz-ipht.de

saturable absorber, which is responsible for the mode-locking. In addition, novel real-time measurement techniques have enabled significantly increased data acquisition rates up to the order of pulse repetition in a laser cavity. The first ultrafast optical Sagnac effect measurement was realized by analyzing real-time spatio-temporal dynamics of ultrashort pulses.^[8] A more sophisticated dispersive Fourier transformation (DFT) technique allows analysis of single-shot pulse spectra in MHz rate. The DFT technique is based on space-time duality: a temporal waveform of an ultrashort pulse transforms into a spectral shape during linear propagation in a dispersive media. In a nutshell, each of the components in the pulse spectrum gets delayed due to the chromatic dispersion and, therefore, arrives separately onto the photodetector. Thus, the DFT technique allows recording of the continuous evolution of pulse spectrum when the dispersive medium fulfills the far-field diffraction condition, i.e., the accumulated dispersion significantly exceeds the initial width of a transform-limited pulse.^[9,10] Many ultrafast phenomena were experimentally revealed by using the DFT measurements, e.g., self-organization of ultrashort coherent structures,^[11,12] spectra pulsations,^[13] and vibration dynamics of bound solitons,^[14] to name a few. Moreover, the DFT technique proved its suitability to characterize phase stability of the ultrashort pulse train^[15] and other practical applications as an all-optical digitizer,^[16] imaging,^[17] displacement sensing,^[18] and LiDAR systems.^[19]

The DFT measurements of counterpropagating pulse in bidirectional fiber lasers demonstrated their complex dynamics of soliton collisions, energy exchanges, and central wavelength drifts and synchronization with a tendency to Q-switched instability or multisoliton operation.^[20–22] Such dynamics are particularly detrimental to gyroscopic measurements. Additionally, previous works on ultrafast laser gyroscopes have indicated that their resolution is strongly limited by the stability of the carrier-envelope phase (CEP).^[6,8] Overall, bidirectional laser systems suffer from a sophisticated cavity design and require subtle adjustment to stabilize the mode-locking operation regime efficiently.

In this work, we propose a combination of advantages of passive FOGs with the benefits of an ultrashort pulse operation regime and real-time measurements. Our simple concept is based on a Mach–Zehnder interferometer (MZI), seeded with the ultrashort soliton train from a conventional unidirectional mode-locked fiber laser. The application of unidirectional laser generation secures high stability of the pulse parameters, which cannot be guaranteed for bidirectional mode-locked operation in active gyroscopes. While propagating over two separate arms of the MZI, complex collision dynamics between the counterpropagated solitons is entirely avoided. Moreover, the MZI design ensures the interference of the pulse with itself. Thus, such configuration helps eliminate the aspect of the carrier-envelope phase stability because the phase fluctuations of the incoming pulses are cancelled out. Furthermore, the setup is insensitive to the timing jitter. The proposed combination of the DFT technique with the ultrashort pulse interferometry for retrieving the phase shift opens the opportunities for simultaneously achieving a high data acquisition rate and measurement precision. The data rate of the gyroscopic measurement, achieved in this work, is ≈ 15 MHz, which is limited by the repetition rate of the used

mode-locked fiber laser. We foresee that the presented configuration has the potential to outperform small-sized active gyroscopes substantially.

To assess the gyroscope performance, we used a stepper motor with adjustable step size and angular velocity (steps per second), which presents a conventional test-bed for investigating the response of the measurements setup, particularly to dynamically varying angular velocities. Overall, this work demonstrates the single-shot phase retrieval resolution of 7.2 mrad, corresponding to a timing shift of 8.6 as an angular velocity of ≈ 0.33 mdeg s^{-1} . The bias instability, i.e., the lowest value of the Allan deviation, of 0.06 deg h^{-1} is achieved at the integration time of 17.07 μs . We have confirmed the acquired phase measurements by extracting the time separation between the pulses encoded in the interferometric pattern. Finally, we have also demonstrated that the suggested gyroscope configuration can measure angular acceleration of each individual step of the motor. We believe that this work provides new insight into phase-based measurements at high acquisition rates and is not limited to only gyroscopic applications.

2. Results and Discussion

The suggested gyroscope configuration is based on MZI, which splits the train of ultrashort pulses into two identical replicas via a 3 dB fiber coupler. The nearly equal length of each arm of the interferometer ensures that the pulse interferes with its replica. Numerically, when both arms of the MZI are coiled with opposite winding paths, the phase of the pulse in each of its arms during the rotation can be expressed as

$$\begin{aligned}\phi_1 &= \delta\phi + \phi_{\text{delay1}} + \phi_{\text{Sagnac}} \\ \phi_2 &= \delta\phi + \phi_{\text{delay2}} - \phi_{\text{Sagnac}}\end{aligned}\quad (1)$$

where $\delta\phi$ is the phase of the pulse at the input of the MZI; ϕ_{delay1} and ϕ_{delay2} are accumulated phases due to propagation in the different arms of the interferometer. The sign of the Sagnac phase shift ϕ_{Sagnac} depends on the direction of the angular rotation. Therefore, the resulting relative phase at the output of the MZI is the difference between the phase of each pulse

$$\Delta\phi = \phi_1 - \phi_2 = \phi_{\text{delay1}} - \phi_{\text{delay2}} + 2\phi_{\text{Sagnac}} = \Delta\phi_{\text{delay}} + 2\phi_{\text{Sagnac}}\quad (2)$$

As can be seen, the relative phase at the output is independent of the phase fluctuations of the incoming pulses. Note, if only one arm of the interferometer is placed on the rotation platform, the Sagnac phase response will not be multiplied by a factor of 2. The phase component $\Delta\phi_{\text{delay}}$ is responsible for the difference between the lengths of both arms of the interferometers and, ideally, remains constant over time. Nevertheless, as the optical path can fluctuate over time, e.g., due to temperature fluctuations, this phase term presents the measurement's primary source of error uncertainty. These fluctuations were strongly suppressed because both arms of the interferometer were placed on the same rotational platform.

Figure 1a demonstrates the recorded DFT spectra of the pulses interference at the output of the MZI, while the gyroscope

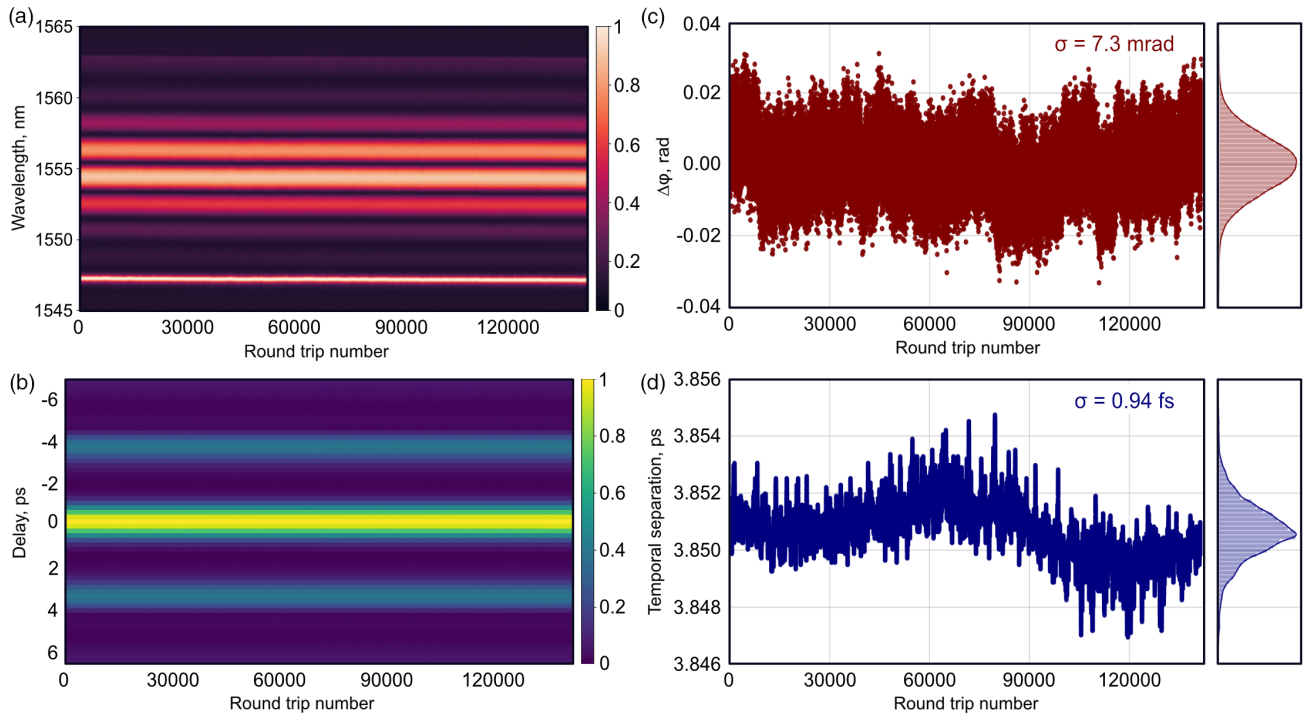


Figure 1. a) The DFT measured spectra from the MZI at rest. b) The single-shot first-order autocorrelation function, numerically obtained from the DFT spectra. c) The single-shot extracted relative phase with corresponding probability density function. The standard deviation is 7.3 mrad. d) Temporal separation between the pulses with moving averaging window of 100 roundtrips.

platform is at rest. The corresponding roundtrip-resolved first-order autocorrelation is shown in Figure 1b, obtained via the fast Fourier transformation from single-shot spectra.^[23] Both figures indicate a stable interference between two pulses with high modulation depth. Figure 1c shows the extracted relative phase from the spectral interferometric pattern with the corresponding probability density function, using the algorithms described in refs. [14,15]. The standard deviation is 7.3 mrad, which corresponds to 8.7 as timing shift at a central wavelength of 1555 nm. The standard deviation defines the smallest distinguishable relative phase change from the noise that equals the resolution of the proposed phase method. Due to the normal distribution, the standard deviation, and the minimum resolution as a consequence, could be further enhanced by \sqrt{n} by averaging over n roundtrips, obeying the normal distribution for white noise. However, the averaging will come at a price of a decreased acquisition rate by n times.

Figure 1d demonstrates the relative timing separation between the pulses from the interferometer with a moving average window of 100 roundtrips, resulting in the temporal resolution of 0.78 fs. The average temporal separation is 3.85 ps with a standard deviation of 0.94 fs. A low value of the standard deviation evidences that the relative phase measurements are not affected by the timing jitter of the laser source. Indeed, the timing jitter is converted into a temporal deviation of the arriving time of the pulse to the MZI input. Nevertheless, due to the time-frequency duality of the DFT measurements, the timing jitter can be interpreted as a uncertainty of the central wavelength of the interferometric pattern, causing additional fluctuations of

the relative phase, as shown in our previous work.^[21] However, this effect is significantly reduced compared to the unidirectional lasers, where the timing jitter is directly converted to the phase fluctuations, as confirmed in our previous studies.^[15]

The timing jitter of the laser source can affect the measurements of the platform acceleration. However, its effect could be neglected because the timing jitter is negligible compared to the roundtrip time. The uncertainty of the angular acceleration measurements due to the timing jitter of the laser source can be estimated as $\Omega_{\text{jitter}} = \tau_{\text{jitter}}/T_{\text{rep}}$. Here, Ω_{jitter} is the uncertainty in the measurements of the angular acceleration due to the timing jitter, τ_{jitter} is the timing jitter, and T_{rep} is the pulse timing period.

We have verified the potential of the proposed real-time technique for gyroscopic measurements by retrieving the phase dynamics of ultrashort pulses during the rotation of the MZI. During the experiments, the stepper motor was attached to the outer edge of the circular platform on which the fiber MZI was placed. So, the rotation was enabled through the friction between the platform and the motor with a gear ration of ≈ 126 . The full step of the motor produces an angular shift of the gyroscopic platform of 7.1 mdeg (124.6 μrad). In the first experiment, the stepper motor was set to the angular velocity of 300 steps per second, corresponding to one step duration of 3.3 ms, or equivalently 50 000 roundtrips of the used 15 MHz ultrafast fiber laser. **Figure 2** demonstrates the characteristic measurements of MZI platform rotation with full- and half-step sizes, which corresponds to the average angular velocity of 2.13 deg s^{-1} (37 mrad s^{-1}) and 1.07 deg s^{-1} (18.6 mrad s^{-1}), respectively. The angular rotations produced the average phase

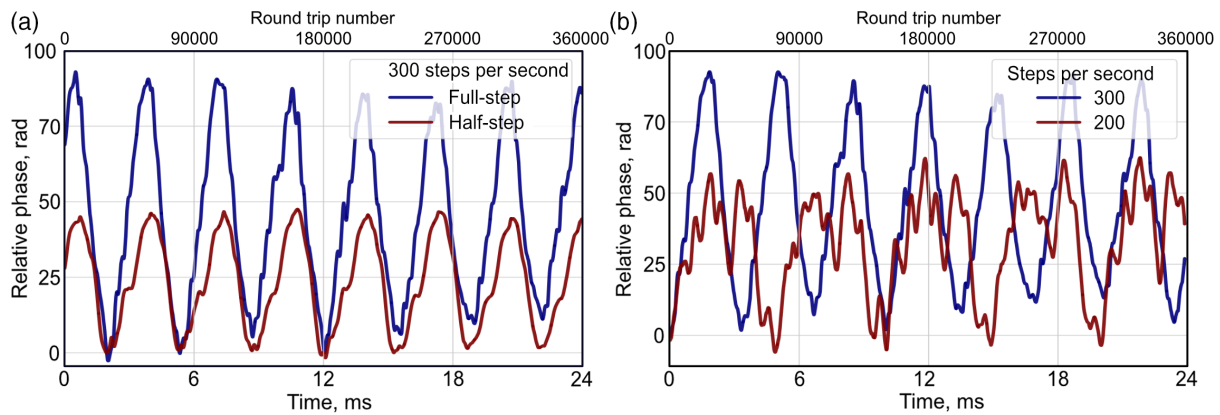


Figure 2. a) Relative phase dynamics under rotational exposure by a stepper motor with full-step (blue line) and half-step size (red line) at 300 steps per second (50 000 roundtrips or 3.33 ms per step). b) Relative phase dynamics under rotational exposure by a stepper motor, set to produce 300 steps per second (blue line) and 200 steps per second (75 000 roundtrips or 5 ms per step; red line) at full-step size.

shift of 47.22 and 23.08 rad, respectively. The recorded step duration is in good agreement with the anticipated value of 3.3 ms per step. Moreover, Figure 2a shows a twofold decrease in phase shift when the stepper motor operates in the half-step regime. We would like to highlight that while replicated series of the experiment have qualitatively confirmed the recorded dynamics, the particular patterns of individual steps could alter due to the slippage between the stepper motor and the rotation platform.

Figure 2b compares the phase measurements at different speeds of the stepper motor. The motor was set to produce 300 and 200 full steps per second, corresponding to the step duration of 3.3 and 5 ms, respectively. The experimental step duration is in good agreement with the expected values. The obtained average phase shift during the platform rotation at the rate of 200 full steps per second is 32.73 rad and 1.44 times smaller than the stepper motor produced 300 steps per second (expected value is 1.5). Figure 2b demonstrates a complex two-peak angular profile of individual motor steps at the setting of 200 steps per second. Such behavior is due to a more extended

switch between the stepper motor's coils. As expected, we have not observed any synchronization dynamics or lock-in effect while investigating the presented passive gyroscope configuration, which confirms that ultrashort pulses could be effectively used for gyroscopic measurement in a passive configuration.

Figure 3a shows a comparison of the relative phase measurements and the relative temporal position between the pulses at the output of the interferometer, extracted from the same interferometric pattern. Note that the zero temporal deviation in Figure 3a corresponds to the temporal separation when the gyroscope was at rest. To plot the relative phase in the time domain, we transformed the phase data using the phase-time relation $\phi = t \cdot \omega$, where ω is the carrier angular frequency of the pulse. The single-shot resolution of the temporal measurements, obtained from the interferogram is 7.8 fs. The average temporal shift is 39.82 fs, corresponding to an error with the phase data of only 4%. Such a good agreement between both measurements supports our results on gyroscopic measurements. Furthermore, both data of relative phase and temporal measurements can be

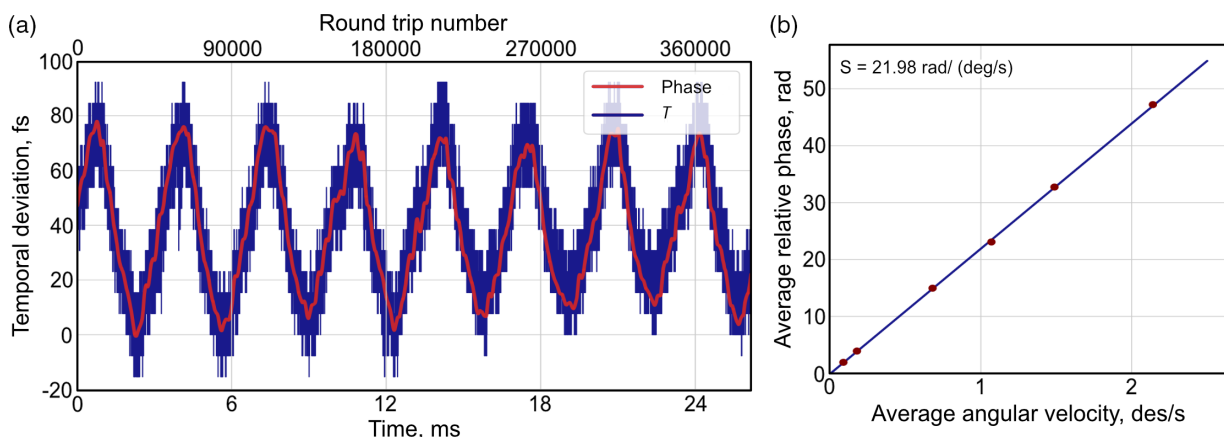


Figure 3. a) Dynamics of the relative phase (red line) and the relative temporal separation (blue line) between the pulses from the interferometer extracted from the same interferometric pattern. The phase data were converted to the temporal domain by using the phase-time relation. The motor was set to produce 300 steps per second at full-step size (50 000 roundtrips or 3.33 ms per step). b) The experimentally obtained relation between applied average angular velocity and the observed average shift in relative phase with linear approximation. The resulting scale factor is 21.98 rad (deg s)⁻¹.

simultaneously used to increase the total resolution of the setup further.

The scale factor of the passive gyroscope configuration was estimated from a linear approximation between the applied average angular velocity and the observed average shift of the relative phase and depicted in Figure 3b. The applied angular rotation ranged from 89.3 mdeg s^{-1} (200 steps per second at 1/16 step size) up to 2.14 deg s^{-1} (300 full steps per second). The resulting scale factor is $21.98 \text{ rad (deg s)}^{-1}$ or $18.02 \text{ fs (deg s)}^{-1}$. Based on this value and the standard deviation of the reference measurements of 7.3 mrad (Figure 1c), the angular velocity resolution in the single-shot regime (at 15 MHz data acquisition rate) is estimated to be 0.33 mdeg s^{-1} ($5.8 \text{ } \mu\text{rad s}^{-1}$).

Here, we would like to note that the experimentally obtained scale factor significantly exceeds the theoretical value based on the Sagnac equations. Earlier works have demonstrated that laser gyroscopes can experience significantly increased Sagnac effect due to nonlinearly induced nonreciprocity,^[24] dispersion,^[25,26] or by operating near exceptional points.^[27,28] To validate the obtained scale factor value, we implemented a few different setups, including 1) an interferometer with a normal dispersion fiber arms; 2) the DFT fiber coil positioned before and after the interferometer; and 3) the DFT spool with different values of the group velocity dispersion (GVD). All of the discussed configurations demonstrate the same scale factor.

The maximum angular velocity, which the suggested setup can detect, is limited by the range of inter-pulse temporal separation, while the interferometric pattern is preserved. As Sagnac effect manifests as a temporal shift, at high angular velocities the pulses could be driven significantly far apart. In such a case, the interferometric pattern could not be resolved due to the limited spectral resolution. This temporal range is estimated to be $\approx 340 \text{ ps}$.^[15] However, to allow the measurement of angular rotations in both directions this value should be halved. For the experimentally obtained scale factor of $18.02 \text{ fs (deg s)}^{-1}$, the maximum velocity is limited to 9.43 kdeg s^{-1} and could be further increased proportionally with the DFT spectral resolution enhancement.

The acceleration of the platform could be calculated by differentiation of the data on angular velocity over roundtrips as shown in Figure 4. The single-shot resolution of the acceleration is defined as the standard deviation divided by the repetition period of the pulse train and equals 4.98 kdeg s^{-2} . However, to resolve the acceleration of the stepper motor, we used a moving averaging window over 1000 roundtrips which provided the resolution of $\approx 5 \text{ deg s}^{-2}$. The theoretically predicted average acceleration during the first half of the step cycle is $2571.4 \text{ deg s}^{-2}$, while the experimentally obtained value is $2253.5 \text{ deg s}^{-2}$. Figure 4 evidences that each step has positive acceleration for a longer period of time than the half of the cycle, while the following deceleration of the platform occurs during the time period shorter than the half-cycle. Thus, the error between the expected and experimental values is mainly attributed to the complex step profile of the stepper motor, which is different from the sine approximation. The resulting average acceleration per step is $-12.7013 \text{ deg s}^{-2}$, which is expected to be close to zero with a residual mistake of 0.56% related to the mean value of acceleration. These measurements of angular acceleration are significant as they provide more information about the dynamics of the platform.

The maximum applied angular acceleration is limited by the periodic nature of the interferometric pattern, so the accumulated Sagnac phase shift per each pulse should not exceed π . Hence, the maximum angular acceleration that could be unambiguously retrieved is determined as the angular velocity corresponding to the phase shift of π divided by the pulse period and is equal to 2.14 Mdeg s^{-2} . The maximum angular acceleration could be further increased by using a pulse train with a higher pulse repetition rate.

Finally, for the full description of the gyroscope performance, we calculated the Allan deviation of the retrieved phase, as shown in Figure 5. The Allan deviation is a traditional approach for estimating noise and stability of oscillating frequency over different time scales and is widely used in optical clock systems, gyroscopes, and other applications where high stability is required.^[29] The maximum integration time of 8.7 ms is limited by the memory depth of the used digital storage oscilloscope. The calculated

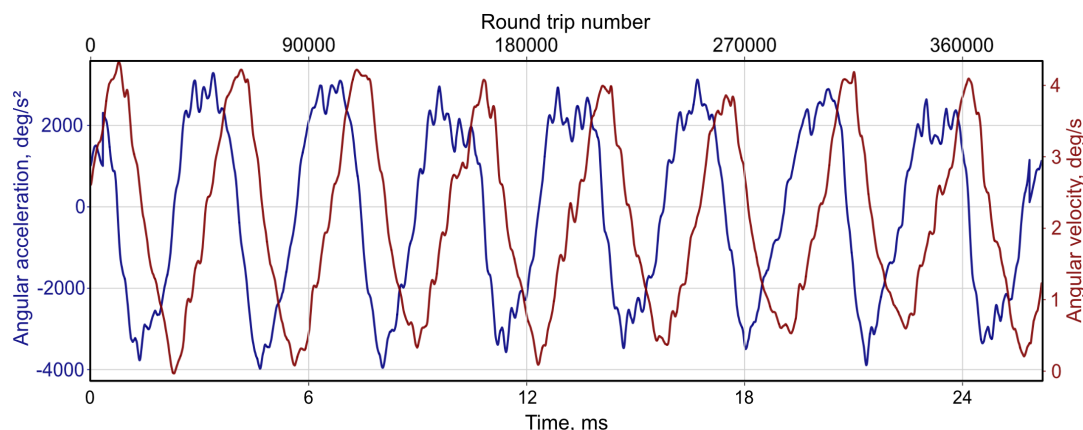


Figure 4. Angular acceleration (blue line) and angular velocity (red line) of the laser platform during rotation exposure by the stepper motor. The motor was set to produce 300 full steps per second (50 000 roundtrips or 3.33 ms per step). The acceleration was obtained by differentiating the velocity over a window of 10 000 roundtrips to increase the resolution.

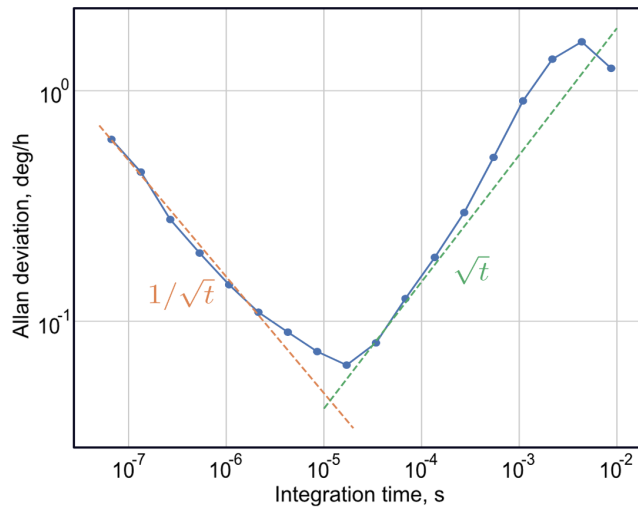


Figure 5. Allan deviation of the relative phase dynamics in a passive gyroscope during the reference measurements.

Allan deviation shows two strong trends, which are related to the noises of the system. The Allan deviation is decreasing with $1/\sqrt{t}$ trend, which is related to the averaging of the white noise. The minimum Allan deviation of 0.06 deg h^{-1} ($0.29 \mu\text{rad s}^{-1}$) is observed at the integration time of $17.07 \mu\text{s}$. So, the maximum resolution could be achieved at the data rate of 58.6 kHz . At the integration time longer than $17 \mu\text{s}$, the Allan deviation starts to increase with a rate of \sqrt{t} due to long-term uncompensated noises.

Such a low value of the bias instability presents a significant improvement when compared to previous results^[5] and is close to meet the requirements set on laser gyros used for navigation purposes.^[30,31] Furthermore, the demonstrated passive gyroscope is able to provide measurements at the data acquisition rate by orders of magnitude higher than demonstrated in other systems.^[5,32–35] The much higher data rate is achieved by processing each consecutive single-shot interferometric pattern recorded via DFT. Such an approach does not require additional integration time compared to the traditional technique based on

beat-note measurements. Therefore, the data rate is only limited by the data rate of the seed ultrafast laser. In such context, for more precise angular acceleration measurements, seed laser sources with a shorter pulse repetition period, such as microcavities,^[32] could be even more beneficial. Still, the scale factor of the MZI interferometer would not get affected by the increased repetition rate because it is governed by the length of the interferometer. This fact manifests an additional advantage over active fiber laser gyroscopes where the increased data rate can be achieved in shorter laser cavities and, thus, will come at the price of the lower resolution due to lower covered area.

3. Conclusion

In this work, we have demonstrated gyroscopic measurements using a passive all-fiber setup, using for the first time, to the best of our knowledge, a MZI seeded by an ultrafast fiber laser. The Sagnac phase shift has been retrieved using real-time DFT measurements of the interferometric signal at a data rate of 15 MHz . The presented DFT setup provides the single-shot phase resolution of 7.3 mrad . Overall, the real-time phase measurements have enabled the single-shot angular velocity resolution of 0.33 mdeg s^{-1} , which has also been confirmed by the simultaneous derivation of the temporal interpulse separation. By measuring the average phase shift at various angular velocities ranging from 89.3 mdeg s^{-1} to 2.14 deg s^{-1} , we have obtained the gyroscope scale factor of $21.98 \text{ rad (deg s)}^{-1}$. We would like to note that the obtained value of the scale factor significantly exceeds the theoretical estimation based on the classical Sagnac equations. The upper limit of angular velocity, which could be retrieved using the presented gyroscopic configuration, is 9.43 kdeg s^{-1} and is limited by the spectral resolution of the DFT measurements. The bias instability, assessed as a minimum value of the Allan deviation, was 0.06 deg h^{-1} at the integration time of $17.07 \mu\text{s}$ (58.6 kHz). Finally, we presented the measurements of the angular acceleration of the rotation platform with the single-shot resolution of 4.98 kdeg s^{-2} , which could be further decreased, inversely proportional to the number of the integrated roundtrips. The upper limit for angular acceleration for the current gyroscope operation is 2.14 Mdeg s^{-2} .

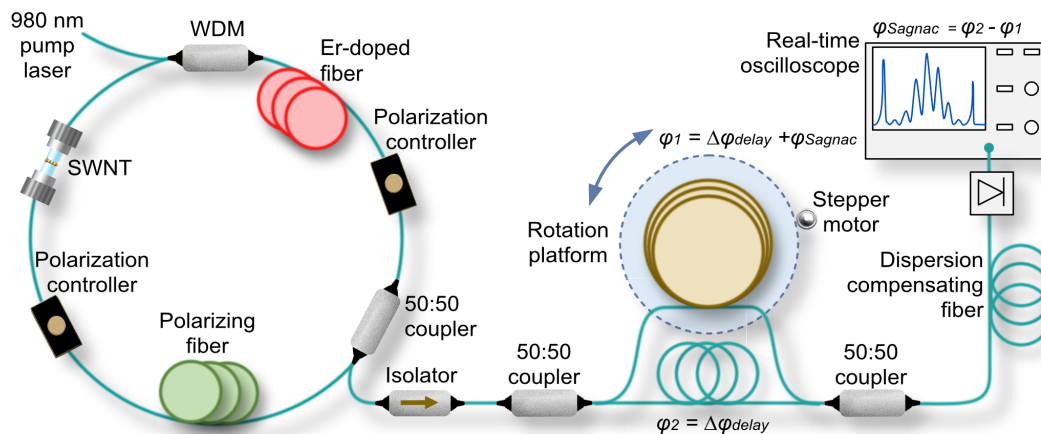


Figure 6. The measurement setup.

The gyroscope constructed as a MZI in combination with analysis of real-time ultrashort pulse dynamics has demonstrated the performance significantly surpassing previous attempts on gyroscopes based on ultrafast fiber lasers. Moreover, the setup is also free from the “lock-in” effect or collision dynamics between the counterpropagating pulses. Our experimental results have confirmed that the MZI-based gyroscope configuration is not affected by seed laser instabilities such as temporal and phase fluctuations of ultrashort pulses. Additionally, active stabilization of the MZI length would further reduce the residual fluctuations and, as a result, enhance angular rotation resolution and reduce Allan deviation over the longer integration time. Another strategy to increase the gyro performance would be the application of polarization-maintaining fibers inside the interferometer. Additionally, a temperature-insensitive interferometer, as suggested in ref. [36], can substantially decrease the influence of the temperature fluctuations on the length of optical paths in MZI arms.

To summarize, the results presented in this article have established that the combination of the DFT technique with interferometric phase measurements is an efficient approach for enabling precision gyroscopic measurements at high data rates. The demonstrated setup can operate over a broad range of applied angular velocities and accelerations. Therefore, we believe that the presented concept of DFT interferometry is not limited only to the gyroscopic measurements, and can be extended to other phase-sensitive applications.

4. Experimental Section

Figure 6 demonstrates the experimental setup of the used mode-locked fiber laser associated with the MZI. The stable generation of ultrashort pulses is achieved using hybrid mode-locking, based on the coaction of a single-walled carbon nanotube saturable absorber and the nonlinear polarization evolution (NPE). The latter is implemented through the section of polarizing fiber (HB1550Z from Thorlabs) and a pair of polarization controllers. While the laser cavity lacked an optical isolator, the unidirectional generation with more than 20 dB extinction ratio is ensured by a proper adjustment of the polarization controllers.^[37] The laser generates 570 fs pulses with the average output power of 1 mW and time-bandwidth product of 0.35 in the clockwise direction at a 15 MHz repetition rate.

The MZI splits the ultrashort pulse train via a 3 dB coupler into two arms with a nearly equal length of 12.7 m with total covered area of 2m². A negligible difference between the lengths of both arms of ≈5 mm is introduced to achieve an appropriate interferometric pattern. The arms' length is close to the seed laser cavity length so that only one pulse is propagating through the interferometer in each direction. This aspect is essential for acquiring continuous and unique data on the Sagnac effect after pulse train replicas are combined via a 3 dB coupler at the MZI output. Should the length of the interferometer arms be shorter than the laser cavity roundtrip, the measurement pattern would consist of periodic intervals when no rotation data is recorded. To minimize further the effect of the temperature fluctuations on the length of MZI arms, they were covered with a foam box. The MZI arms are coiled and positioned close to the edge rotation platform with a diameter ≈62 cm to perform the angular velocity measurements.

The DFT line consists of an 11 km dispersion compensating fiber (WBDK-70-L from OFS) with a total group velocity dispersion $D = -1200 \text{ ps nm}^{-1}$ at 1555 nm. The optical signal is recorded by a 50 GHz photodiode (Finisar XPDV2320R) and a 33 GHz 80 GSa s⁻¹ digital storage oscilloscope (Agilent DSOX93204A). The spectral resolution of the DFT measurement, as limited by the bandwidth of the used photodiode and the oscilloscope, is 0.021 nm.^[9]

Acknowledgements

Open Access funding enabled and organized by Projekt DEAL.

Conflict of Interest

The authors declare no conflict of interest.

Data Availability Statement

The data that support the findings of this study are openly available in figshare at <http://doi.org/10.6084/m9.figshare.19430615>, reference number 19430615.

Keywords

dispersive Fourier transformation, fiber-optic gyroscopes, optical Sagnac effect, phase, ultrafast laser

Received: March 28, 2022

Revised: May 17, 2022

Published online:

- [1] A. Pancha, T. Webb, G. Stedman, D. McLeod, K. Schreiber, *Geophys. Res. Lett.* **2000**, *27*, 3553.
- [2] K. U. Schreiber, T. Klügel, J.-P. R. Wells, R. B. Hurst, A. Gebauer, *Phys. Rev. Lett.* **2011**, *107*, 173904.
- [3] G. Sagnac, *C.R. Acad. Sci.* **1913**, *157*, 1410.
- [4] F. Aronowitz, R. Collins, *Appl. Phys. Lett.* **1966**, *9*, 55.
- [5] I. Kudelin, S. Sugavanam, M. Chernysheva, *Sensors* **2021**, *21*, 3530.
- [6] A. A. Krylov, D. S. Chernykh, E. D. Obratsova, *Opt. Lett.* **2017**, *42*, 2439.
- [7] J. Chesnoy, *Opt. Lett.* **1989**, *14*, 990.
- [8] M. Chernysheva, S. Sugavanam, S. Turitsyn, *APL Photonics* **2020**, *5*, 016104.
- [9] K. Goda, B. Jalali, *Nat. Photonics* **2013**, *7*, 102.
- [10] A. Mahjoubfar, D. V. Churkin, S. Barland, N. Broderick, S. K. Turitsyn, B. Jalali, *Nat. Photonics* **2017**, *11*, 341.
- [11] G. Herink, B. Jalali, C. Ropers, D. Solli, *Nat. Photonics* **2016**, *10*, 321.
- [12] J. Peng, M. Sorokina, S. Sugavanam, N. Tarasov, D. V. Churkin, S. K. Turitsyn, H. Zeng, *Commun. Phys.* **2018**, *1*, 20.
- [13] M. Liu, Z.-W. Wei, H. Li, T.-J. Li, A.-P. Luo, W.-C. Xu, Z.-C. Luo, *Laser Photonics Rev.* **2020**, *14*.
- [14] Z. Wang, K. Nithyanandan, A. Coillet, P. Tchofo-Dinda, P. Grelu, *Nat. Commun.* **2019**, *10*, 830.
- [15] I. Kudelin, S. Sugavanam, M. Chernysheva, *Opt. Express* **2021**, *29*, 18734.
- [16] A. Fard, B. Buckley, S. Zlatanovic, C.-S. Bres, S. Radic, B. Jalali, *Appl. Phys. Lett.* **2012**, *101*, 051113.
- [17] K. Goda, A. Ayazi, D. R. Gossett, J. Sadasivam, C. K. Lonappan, E. Sollier, A. M. Fard, S. C. Hur, J. Adam, C. Murray, C. Wang, N. Brackbill, D. Di Carlo, B. Jalali, *Proc. Natl. Acad. Sci.* **2012**, *109*, 11630.
- [18] K. Goda, K. K. Tsia, B. Jalali, *Appl. Phys. Lett.* **2008**, *93*, 131109.
- [19] Y. Jiang, S. Karpf, B. Jalali, *Nat. Photonics* **2020**, *14*, 14.
- [20] I. Kudelin, S. Sugavanam, M. Chernysheva, *Photon. Res.* **2020**, *8*, 776.
- [21] I. Kudelin, S. Sugavanam, M. Chernysheva, *Commun. Phys.* **2020**, *3*, 1.
- [22] Z. Wang, Q. Jiang, Z. Tang, Z. Zhang, *Opt. Express* **2020**, *28*, 28209.
- [23] G. Herink, F. Kurtz, B. Jalali, D. Solli, C. Ropers, *Science* **2017**, *356*, 50.
- [24] A. Kaplan, P. Meystre, *Opt. Lett.* **1981**, *6*, 590.

- [25] J. Hendrie, M. Lenzner, H. Afkhamiardakani, J. C. Diels, L. Arissian, *Opt. Express* **2016**, *24*, 30402.
- [26] D. D. Smith, H. Chang, L. Arissian, J. C. Diels, *Phys. Rev. A* **2008**, *78*, 053824.
- [27] Y.-H. Lai, Y.-K. Lu, M.-G. Suh, Z. Yuan, K. Vahala, *Nature* **2019**, *576*, 65.
- [28] S. Sunada, *Phys. Rev. A* **2017**, *96*, 033842.
- [29] O. J. Woodman, An Introduction to Inertial Navigation, Technical report, University of Cambridge, Computer Laboratory, UK **2007**.
- [30] W. Chow, J. Gea-Banacloche, L. Pedrotti, V. Sanders, W. Schleich, M. Scully, *Rev. Mod. Phys.* **1985**, *57*, 61.
- [31] A. Braga, J.-C. Diels, R. Jain, R. Kay, L. Wang, *Opt. Lett.* **2010**, *35*, 2648.
- [32] Y.-H. Lai, Y.-K. Lu, M.-G. Suh, Z. Yuan, K. Vahala, *Nature* **2019**, *576*, 65.
- [33] V. Passaro, A. Cuccovillo, L. Vaiani, M. De Carlo, C. E. Campanella, *Sensors* **2017**, *17*, 2284.
- [34] D. T. Mead, S. Mosor, *Optical Waveguide and Laser Sensors*, Vol. 11405, International Society for Optics and Photonics **2020**, p. 1140509.
- [35] K. Carr, R. Greer, M. B. May, S. Gift, in *2014 IEEE/ION Position, Location and Navigation Symp.-PLANS 2014*, IEEE, Piscataway, NJ **2014**, pp. 1392–1408.
- [36] W. Zhu, E. R. N. Fokoua, Y. Chen, T. Bradley, M. N. Petrovich, F. Poletti, M. Zhao, D. J. Richardson, R. Slavík, *Opt. Lett.* **2019**, *44*, 2768.
- [37] M. Chernysheva, M. Al Araimi, H. Kbashi, R. Arif, S. V. Sergeyev, A. Rozhin, *Opt. Express* **2016**, *24*, 15721.